Journal of ELECTRONIC MATERIALS, Vol. 47, No. 8, 2018
https://doi.org/10.1007/s11664-018-6375-6

Porous $Ba_{0.85}Ca_{0.15}Zr_{0.1}Ti_{0.9}O_3$ Ceramics for Pyroelectric Applications

MOOLCHAND SHARMA,[1,5] V.P. SINGH,[2] SHATRUGHAN SINGH,[1] PUNEET AZAD,[3] BOURAOUI ILAHI,[4] and NIYAZ AHAMAD MADHAR[4]

1.—IILM - College of Engineering and Technology, Greater Noida 201306, India. 2.—School of Engineering, Indian Institute of Technology Mandi, Mandi, Himachal Pradesh 175005, India. 3.—Department of Electronics and Communication Engineering, Maharaja Surajmal Institute of Technology, C-4, JanakPuri, New Delhi 110058, India. 4.—Department of Physics and Astronomy, College of Sciences, King Saud University, Riyadh 11451, Kingdom of Saudi Arabia. 5.—e-mail: sharma.moolchand09@gmail.com

Porous $Ba_{0.85}Ca_{0.15}Zr_{0.1}Ti_{0.9}O_3$ (BCZT) ferroelectric ceramics were fabricated using a solid-state reaction consisting of BCZT and poly(methyl methacrylate)(PMMA) (2%, 4%, 8% and 10% by wt.%) as a pore former. By increasing the PMMA content from 0% to 10%, porosity increased from 8% to 29%. It was found that the dielectric constant (ε_r) decreased and the dielectric loss ($\tan\delta$) increased with increasing porosity. At 29% porosity, ε_r of the BCZT was found to decrease more, from 3481 to 1117 at 5 kHz and at room temperature. The dielectric constant and volume-specific heat capacity decreased with the increase in porosity which ultimately improved the pyroelectric figure-of-merits (FOMs). Further, the pyroelectric FOMs were estimated and found to be improved at optimum porosity.

Key words: Lead-free, porous, pyroelectric, dielectric

INTRODUCTION

Pyroelectric materials are able to convert time-dependent thermal energy into electrical signals which have been incorporated into various devices.[1–7] Pyroelectric materials are known for their use as uncooled infrared detectors such as night vision googles.[8,9] Pyroelectric-based IR (infrared) detectors have advantages over other IR-based technologies, e.g., high sensitivity, low power requirement, low cost and consistent performance in a wide temperature range. Thermal energy harvesting is another promising area where these materials demonstrate some advantages over Seebeck effect-based thermoelectric materials.[10,11] However, both the phenomena have low conversion efficiency. These materials have also been widely investigated for their electrocaloric effect which is the conversion of electric energy into refrigeration.[12–14] Hundreds of dielectric materials have been documented in the pyroelectric family.[15,16] In order to achieve enhance the performance of pyroelectric materials, there should be a large pyroelectric coefficient, a low dielectric constant and optimum thermal properties.[17–19] These properties can be tuned using physical/chemical adjustments.[20–24] Composites are one of the plausible solutions for altering the above-mentioned physical properties. In this direction, porous pyroelectric ceramics can be a promising solution for thermal sensing applications.[25–28] Porous ceramics can be fabricated using volatile compounds such as carbon-based materials.[28–31] In this context, a few studies have been reported on the dielectric and pyroelectric properties of porous lead-based ceramics.[32] Thus, Zhang et al. fabricated porous pyroelectric ceramics using stearic acid.[31] The porous samples exhibited improved pyroelectric figure-of-merits (FOMs).[33,34] Few lead-free porous ceramics have been reported such as $Ba_{0.5}Sr_{0.5}TiO_3$ and $Ba_{0.67}Sr_{0.33}TiO_3$which showed enhanced FOMs.[18,19,25,26,35] Table I reports the performance of porous pyroelectric ceramics,

(Received February 10, 2018; accepted May 9, 2018; published online May 22, 2018)

Table I. FOMs of well-known porous ceramics at near room temperature

Material	PFA/method	wt.%	% porosity	P ($\mu C/m^2$ K)	ε_r	F_d (10^{-5} $Pa^{-0.5}$)	F_v ($\mu C/m^2$ K)	F_e (pJ/m^3 K^2)	F_e^* (pm^3/J)	References
$Ba_{0.67}Sr_{0.33}TiO_3$	(i) PMMA	0	–	5500	12000	11	–	–	–	25
	(ii) CNT	3	9.6	7000	8000	26	–	–	–	25
		0.6	9.5	7100	8000	27.5	–	–	–	25
		1.2	19.2	3500	4500	11	–	–	–	25
$Ba_{0.67}Sr_{0.33}TiO_3$	PMMA	0	–	5500	12000	11	–	–	–	18
		1	4.7	7000	10000	15	–	–	–	18
		3	9.6	7100	8000	26	–	–	–	18
		6	19.6	3500	5000	8	–	–	–	18
$PbZr_{0.45}Ti_{0.55}O_3$	(i) High M.W. polymer	–	–	215	784	–	0.28	–	–	33
(thin film)	(ii) Low M.W. Polymer	–	25	119	127	–	0.94	–	–	33
		–	21	150	144	–	1	–	–	33
$PbZr_{0.15}Ti_{0.85}O_3$	Low M.W.Polymer	–	–	205	230	–	0.88	–	–	33
(thin film)		–	20	180	91	–	1.92	–	–	33
$Pb(Zr_{0.3}Ti_{0.7})O_3$	70 nm thick	–	–	211	372	1.02	–	–	–	34
	140 nm thick	–	–	236	356	1.62	–	–	–	34
	350 nm thick	–	–	160	210	1.32	–	–	–	34
PZT	Freeze	–	3	391	–	–	–	11.41	1.94	48
	Cast (ice)	–	25	316	–	–	–	11.6	3	48
		–	35	280	–	–	–	12	4.5	48
		–	45	269	–	–	–	12.43	6.57	48
$Bi_{0.5}(Na_{0.82}K_{0.18)0.5}TiO_3$	Ethyl cellulose	–	0	460	600	1.1	–	–	–	49
(thick films)		–	19	440	200	3.5	–	–	–	49
		–	32	420	50	3.8	–	–	–	49
$Pb_{1-x}Ca_xTiO_3$ (x = 0–0.3) (thin film)	Heating rate	–	–	–	–	–	0.5–3.2	–	–	50
$Pb_{1-x}Ca_xTiO_3$ (x = 0–0.3) (thin film)	Heating rate	–	–	–	–	80–140	–	–	–	51

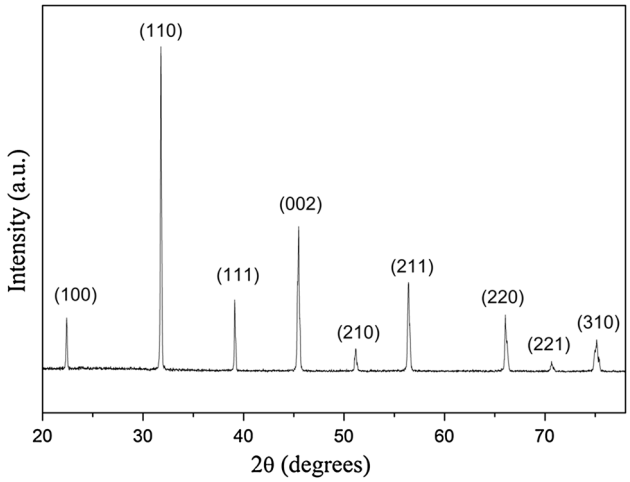

Fig. 1. X-ray diffraction pattern of BCZT ceramic.

from which it is clear that pyroelectric porous ceramics have a limited literature and warrant further research. $Ba_{0.85}Ca_{0.15}Zr_{0.1}Ti_{0.9}O_3$ (BCZT) is one of the promising pyroelectric ceramics which has a significantly high pyroelectric coefficient (p) along with many other promising ferroelectric and piezoelectric properties.[4,21] BCZT has a p value of 7×10^{-4} C/m^2 K at room temperature,[36] and has a piezoelectric coefficient of 630 pC/N.[37] BCZT ceramics could be a promising material for various dielectric applications. In order to further explore this material, we have fabricated porous BCZT ceramics for pyroelectric examination which is discussed in subsequent sections.

EXPERIMENTAL

BCZT powder (along with PMMA, 0 wt.%, 2 wt.%, 4 wt.%, 8 wt.% and 10 wt.%) was prepared using the solid-state reaction route. A stoichiometric ratio of $BaCO_3$ (barium carbonate), CaO (calcium oxide), ZrO_2 (zirconium oxide) and TiO_2 (titanium dioxide) powders was thoroughly mixed and then calcined at 1350°C for 6 h. The powder (mixed with PMMA) was pressed into 12-mm pellets. Calcination and sintering conditions were adopted from the literature.[26] The initial temperature was raised up to 240°C by a step size of 2°C/min. The temperature was further raised to 420°C at 1°C/min and then raised to 850°C at a 2°C/min scan rate to assure the slow burnout of PMMA. The samples were finally sintered at 1450°C for 6 h.

X-ray diffractometry (XRD) with CuKα radiation was used to confirm phase formation. Scanning electron microscopy (SEM) (FEI-Technai SEM, Sirion) was used to capture the surface morphology. The density of the samples was measured with the help of the Archimedes principle-based technique. Ferroelectric hysteresis loops were traced at 50 Hz at various temperatures using a modified Sawyer–Tower circuit. The capacitance of all the compositions was recorded with impedance spectroscopy which was used to calculate the dielectric constants of all the investigated samples.

RESULTS

Figure 1 depicts the XRD pattern of BCZT powder calcined at 1350°C/6 h. Figure 2a–e presents the SEM images of sintered BCZT samples for different wt.% of PMMA. Energy-dispersive x-ray spectroscopy analysis was performed to check the residual carbon traces present in the porous region of the samples (not shown here). Very little trace of carbon ($\sim$ 0.16 wt.%) was found in any of the samples. No correlation was found between the residual carbon and the PMMA (wt.%) added to the samples. This residual carbon may slightly influence the property while it would not affect the relative property of the samples along with PMMA/porosity. Figure 3 presents the relative density of the samples with different PMMA contents. For a constant sintering temperature, from both studies (SEM and density measurements), the porosity was found to be increase when the content of PMMA increased. BCZT exhibited a density of 5.4 g/cm^3 and decreased to 4.2 g/cm^3 at 10% PMMA addition, which is 71% of the theoretical density.

The ferroelectric hysteresis plots were recorded at 303 K, as depicted in Fig. 4a. The pure BCZT ($\alpha = 0$) ceramic exhibited a maximum polarization of 16 μC/cm^2. With an increase in porosity, the saturation polarization decreased, which is an obvious trend. Furthermore, in order to study the temperature dependence of polarization, P–E loops are shown exemplarily in Fig. 4b–e for α = 0–10% at a temperature ranging from 303 K to 393 K. The intensity of polarization decreases with increasing porosity as there is a decrease in the overall volume fraction of the ferroelectric BCZT proportion with the increasing value of α. Also, we can observe a decrease in remnant polarization (P_r) when the PMMA wt.% increases, as observed in Fig. 4a. Figure 5a–g presents the plots of ε_r and tanδ at 303 K/5 kHz with different content of pore former. It can be concluded that the dielectric constant decreases and tanδ increases with increases in porosity.

DISCUSSION

PMMA starts burning above 240°C and this ends at 420°C. In this study, instead of using PVA (polyvinyl alcohol), PMMA solution in acetone has

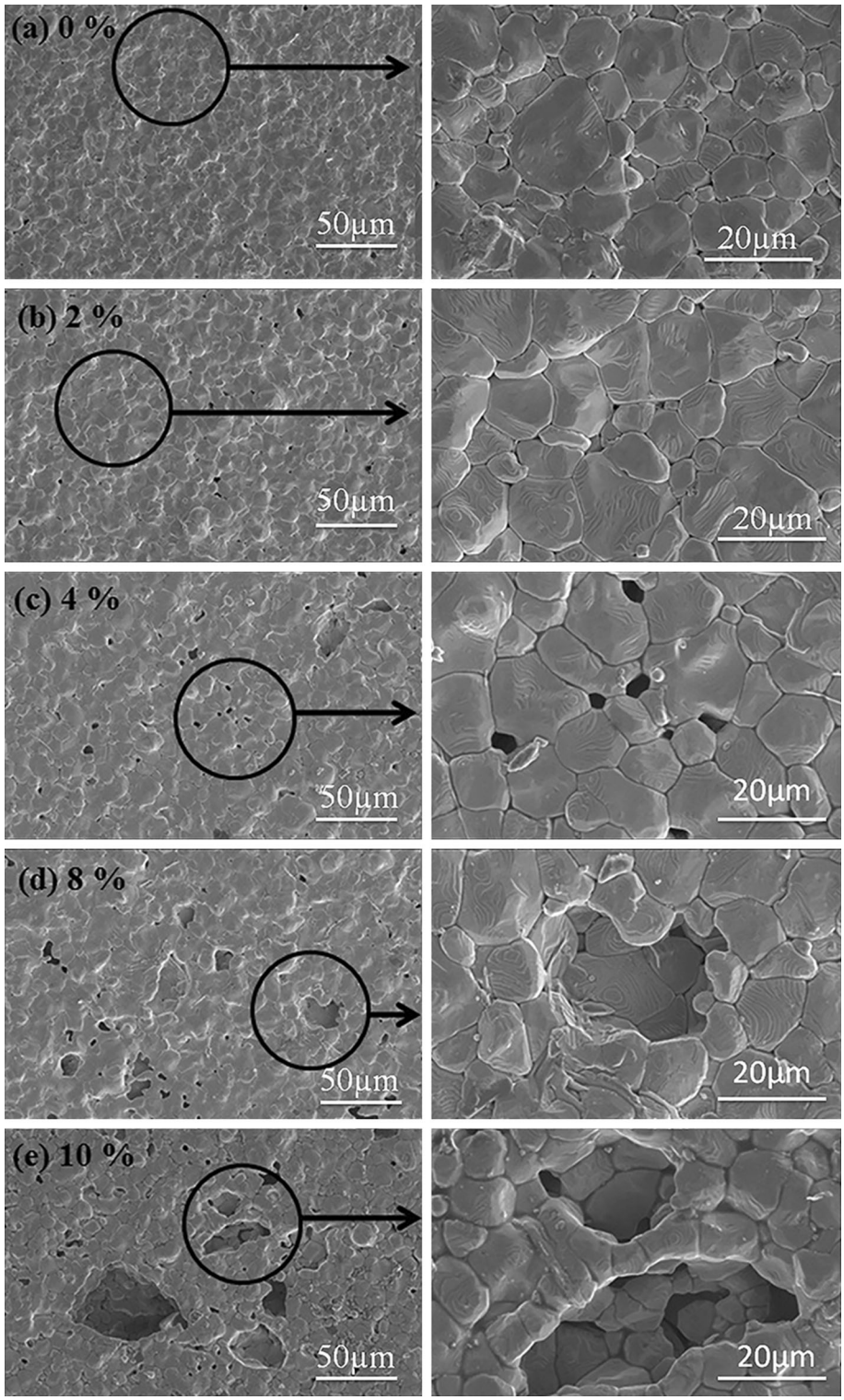

Fig. 2. Scanning electron micrographs of BCZT ceramics with different contents of PMMA: (a) BCZT, (b) BCZT + 2%PMMA, (c) BCZT + 4%PMMA, (d) BCZT + 8%PMMA, and (e) BCZT + 10%PMMA.

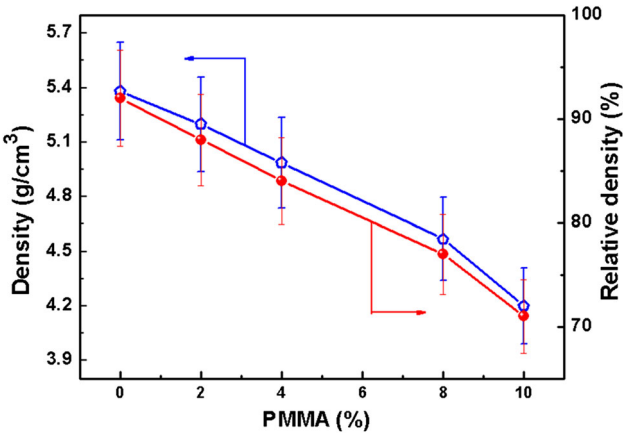

Fig. 3. Variation of density with the content of PMMA as a pore former.

been used as a binder as well as a pore-forming agent. The acetone is able to vaporize during the excessive mixing with the powder and only the uniform dispersion of PMMA remained in the powder. At very low amounts of PMMA, it works as a binder in green pellets. However, using a higher concentration and heating, it starts burning which creates pores in the samples. The result of density measurement and SEM analysis shows the control on porosity as well as the pore size obtained by simply adding different contents of PMMA as a binder. Furthermore, Fig. 5 presents the temperature dependence of the relative dielectric constant and loss at various frequencies for samples having (b) dense BCZT, (c) 2% PMMA, (d) 4% PMMA, (e) 8% PMMA and (f) 10% PMMA. These results are in good agreement with their corresponding ε_r which shows a steady decline with porosity.

Figure 6 shows the pyroelectric coefficient (p) of BCZT-aPMMA (a = 0–10%) plotted against operating temperature for various wt.% of PMMA. Considering the hysteresis P–E loops shown in Fig. 4, the remnant polarization were extracted to study the porosity effect on BCZT ceramics. These P_r values were further exploited to evaluate the pyroelectric coefficient of all the samples using a static method, as shown in Eq. 1:

$$p = \frac{dP_r}{dT} \tag{1}$$

The pyroelectric coefficient also decreases as the porosity increases, as expected. This decrease in p value is due to fact that the porous ceramics is a kind of air–ceramic composite. As air is not a pyroelectric material, overall pyroelectric properties decrease in porous ceramics. Porosity can also induce stress concentrations near pores. It is also well established that stress can alter polarization, which leads to changes in dielectric and pyroelectric properties.[38]

In order to estimate the FOMs, the temperature dependence of the dielectric constant and dielectric loss at the fixed frequency of 5 kHz is depicted in Fig. 5g. There are few FOMs suggested for specific pyroelectric devices. The FOM for current responsivity (F_i) can be expressed as $F_i = \frac{p}{C_v}$ where c_v is the specific heat capacity.[39,40] As the heat capacity of pores is much lower than that of dense ceramics, c_v of pthe orous BCZT ceramics can be represented as[11]:

$$c_v = c_{v(\text{dense})} * (1 - \Phi) \tag{2}$$

where Φ denotes the porosity fraction. Temperature-dependent $c_{v\ (\text{dense})}$ is borrowed from the literature.[41] A decreasing trend in F_i with porosity is observed, as shown in Fig. 7a, which is not a favorable finding. Furthermore, to obtain the maximum voltage for an incident heat input, the FOM governing voltage is $(F_v) = \frac{p}{C_v \varepsilon_r \varepsilon_0}$, where ε_0 and ε_r are the permittivity of vacuum and dielectric constant, respectively.[20,42] F_v increases with porosity due to the direct impact of decreasing two parameters (c_v and ε_r). Likewise, the FOM for a pyroelectric detector application is $(F_d) = \frac{p}{C_v \sqrt{\varepsilon_r \varepsilon_0 \tan\delta}}$.[43,44] Energy-harvesting FOMs $(F_e) = \frac{p^2}{\varepsilon_r \varepsilon_0}$ and $(F_e^*) = (F_i * F_v)$ have been proposed in the literature.[42,45] Temperature-dependent FOMs are shown in Fig. 7. It can be inferred from such studies that both F_e and F_e^* become larger when the porosity is beyond 8% which arises due to the reduced dielectric constant at higher porosity playing a dominant role in switching the FOMs. Furthermore, we have also

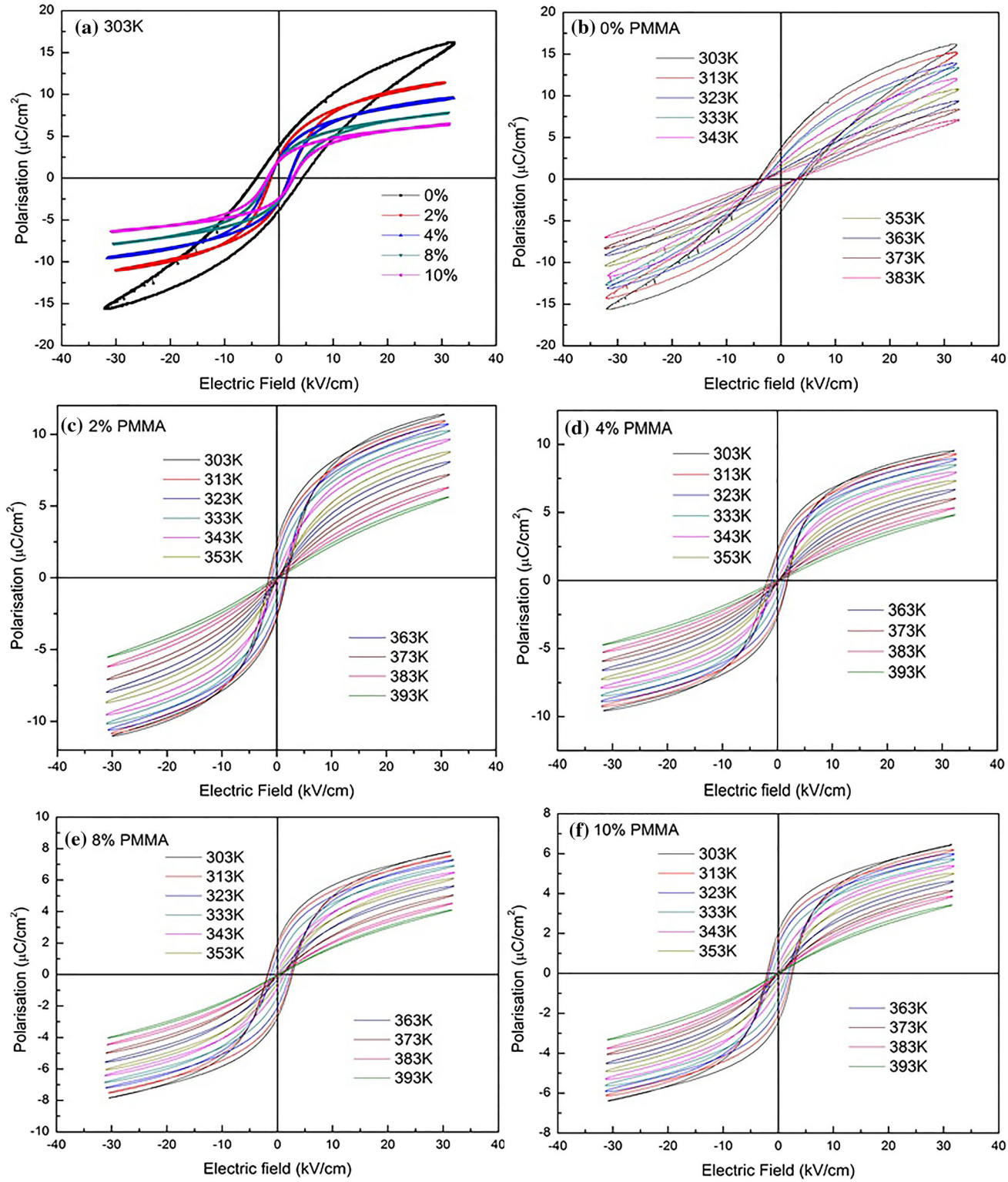

Fig. 4. Polarization–electric field (P–E) hysteresis loops of BCZT ceramic with different contents of PMMA: (a) comparison at 303 K, (b) BCZT, (c) BCZT + 2%PMMA, (d) BCZT + 4%PMMA, (e) BCZT + 8%PMMA, and (f) BCZT + 10%PMMA.

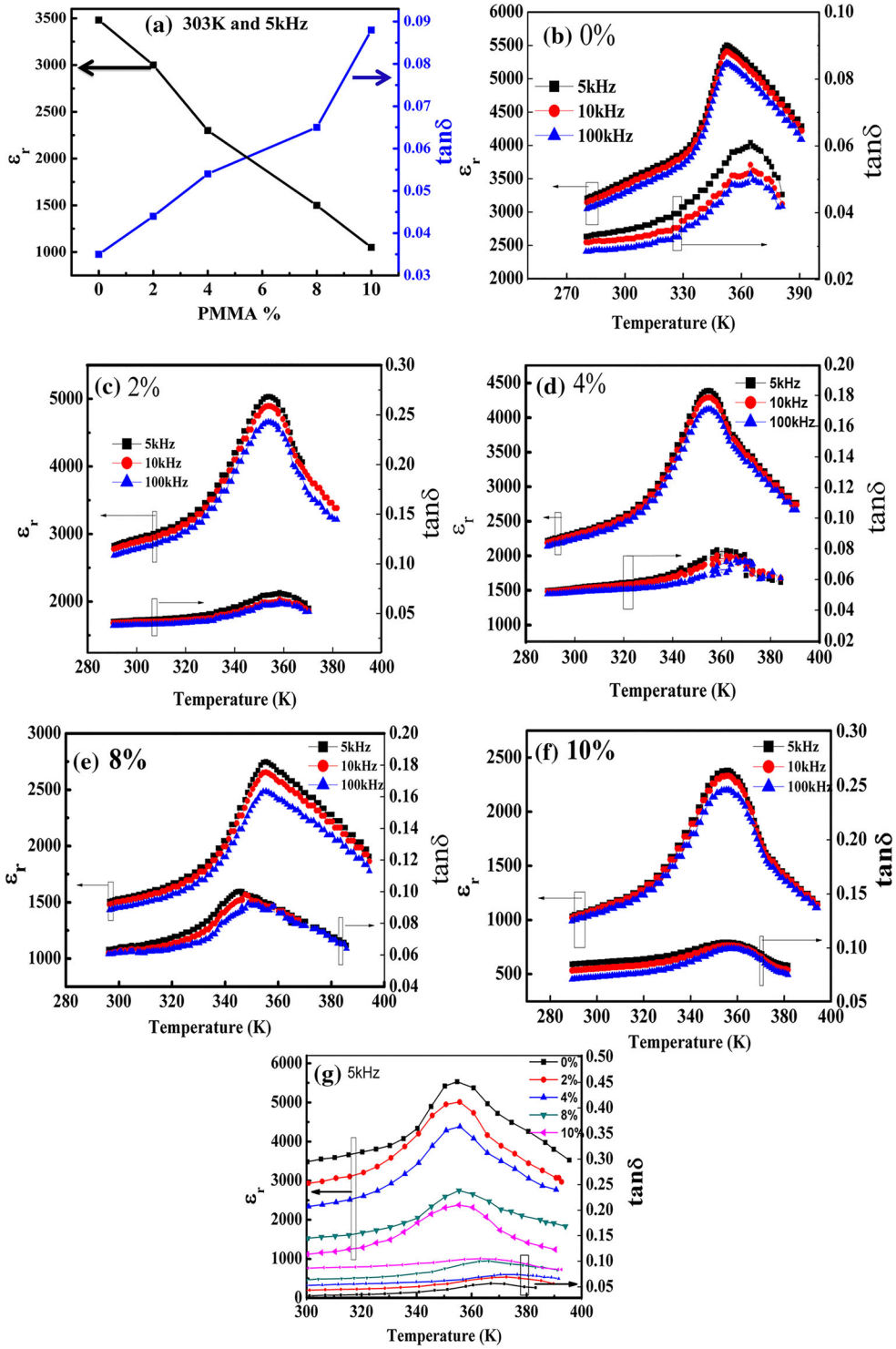

Fig. 5. Temperature dependence of dielectric constant and loss tangent with different porosity: (a) comparison at 303 K/5 kHz, (b) BCZT, (c) BCZT + 2%PMMA, (d) BCZT + 4%PMMA, (e) BCZT + 8%PMMA, (f) BCZT + 10%PMMA, and (g) comparison at 5 kHz.

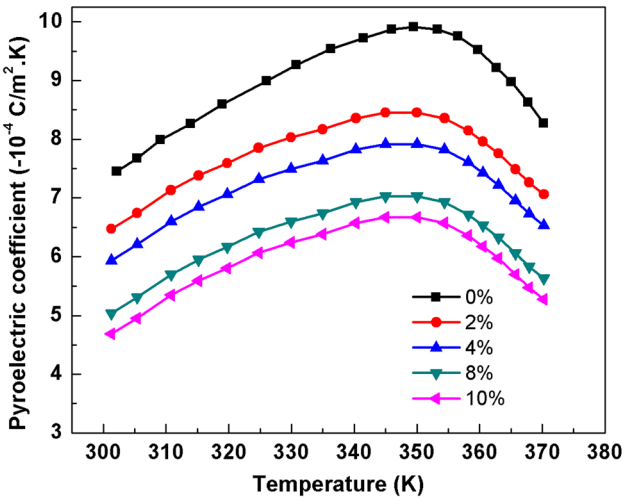

Fig. 6. Pyroelectric coefficient as a function of temperature of all samples with different wt.% of PMMA as a pore former.

plotted all the FOMs at room temperature, as depicted in Fig. 7f–h. For assessing the performance of porous BCZT in relation to other known pyroelectric materials, Table II lists the comparison of results from the literature along with results from the present study.

CONCLUSIONS

The dielectric constant of BCZT reduced as the porosity increased from 8% to 29%. At 29% porosity, ε_r of the BCZT composition decreased by more than 68% at 5 kHz and 303 K. A FOM for voltage responsivity (F_v) showed an 83% improvement over dense ceramics for BCZT10% PMMA sample. Similarly, the maximum FOMs for energy harvesting are F_e (20.1 J/m^{3}K^2) and F_e^*(5.6 pm^3/J) for 10% PMMA, showing around 15% enhancement.

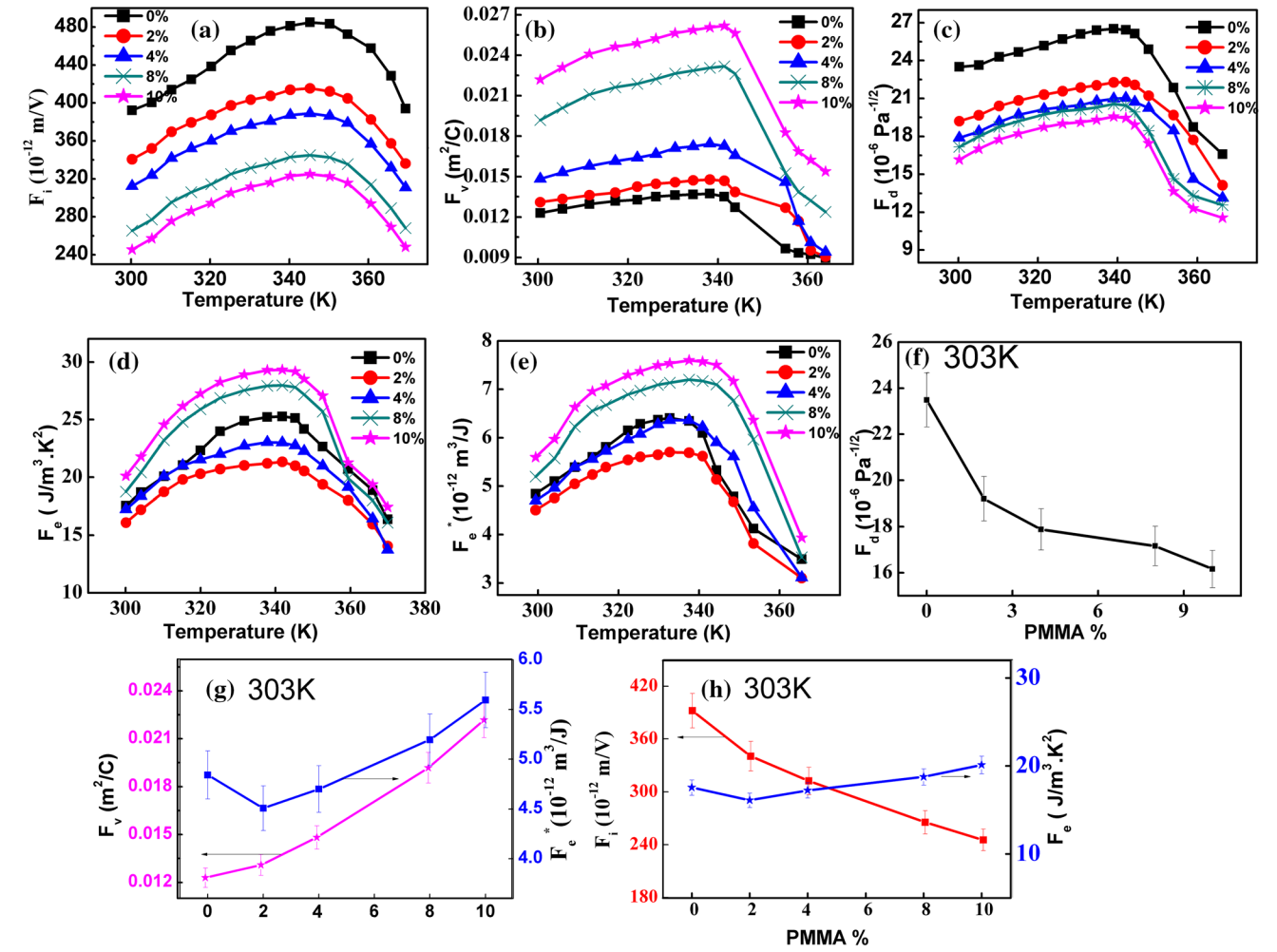

Fig. 7. Plots of FOMs for (a) current responsivity (F_i), (b) voltage responsivity (F_v), (c) detectivity, (d) energy harvesting (F_e) and (e) energy harvesting (F_e^*). (f, g, and h) Comparison at 303 K.

Table II. Comparison of pyroelectric FOMs for well-known lead-free ceramics with porous BCZT-ceramics at room temperature

Material	ε	p (μC/m^2 K)	F_i (p m/V)	F_v (m^2/C)	F_g (J/m^{3}K^2)	F_g^* (pm^3/J)	References
$Ba_{0.85}Ca_{0.15}Zr_{0.1}Ti_{0.9}O_3$ (0% PMMA)	3500	750	390	0.012	17.5	4.8	This work
$Ba_{0.85}Ca_{0.15}Zr_{0.1}Ti_{0.9}O_3$ (8% PMMA)	1500	500	270	0.018	18.7	5.2	This work
$Ba_{0.85}Ca_{0.15}Zr_{0.1}Ti_{0.9}O_3$ (10% PMMA)	1150	470	240	0.022	20.1	5.6	This work
$[(K_{0.5}Na_{0.5})0.96Li_{0.04}]Nb_{0.84}Ta_{0.1}\ Sb_{0.06}O_3$	1520	190	42	0.003	3	0.1	1
$[(K_{0.5}Na_{0.5})0.96Li_{0.04}]Nb_{0.8}Ta_{0.2}O_3$	1230	165	62	0.006	2.8	0.4	1
$BaTiO_3$	1200	200	80	0.008	4.3	0.6	17
$[Bi_{0.5}(Na_{0.95}K_{0.05})_{0.5}]_{0.95}\ Ba_{0.05}TiO_3$	853	325	112	0.015	15.8	1.7	1
Triglycinesulphide (TGS)*	38	280	121	0.362	263.2	44.1	36
Mn:94.6$Na_{0.5}Bi_{0.5}TiO_3$-5.4$BaTiO_3$ [001]*	835	380	131	0.082	22	2.3	43
$NaNO_2$	4	40	18.2	0.514	51	9.3	36
P(VDF-TrFE) 80/20	7	31	13	0.218	17.5	2.9	36
$LiNbO_3$	28.7	83	35	0.141	30.6	6	17
$Ca_{0.15}(Sr_{0.5}Ba_{0.5})Nb_2O_6$	972	361	171	0.02	17.1	3.4	46
$Sr_{0.5}Ba_{0.5}Nb_2O_6$	400	550	239	0.068	96.4	16.2	36
$(Ba_{0.84}Ca_{0.15}Sr_{0.01})(Ti_{0.9}Zr_{0.09}Sn_{0.01})O_3$	4200	1167	479	0.013	33.4	6.21	47

*Single crystal.

ACKNOWLEDGEMENT

The authors would like to extend their sincere appreciation to the Deanship of Scientific Research at King Saud University for funding this research Group No. RG-1436-014.

REFERENCES

1. S.T. Lau, C.H. Cheng, S.H. Choy, D.M. Lin, K.W. Kwok, and H.L.W. Chan, *J. Appl. Phys.* 103, 104105 (2008).
2. S. Bauer and B. Ploss, *J. Appl. Phys.* 68, 6361 (1990).
3. R.W. Whatmore, *Rep. Prog. Phys.* 49, 1335 (1986).
4. S. Patel, A. Chauhan, and R. Vaish, *Int. J. Appl. Ceram. Technol.* 12, 899 (2015).
5. K.S. Srikanth, S. Patel, S. Steiner, and R. Vaish, *Scr. Mater* 146, 146 (2018).
6. S. Patel, D. Sharma, A. Singh, and R. Vaish, *J. Materiomics* 2, 75 (2016).
7. R. Vaish, *Int. J. Appl. Ceram. Technol.* 10, 682 (2013).
8. G. Zhang, S. Jiang, Y. Zhang, and T. Xie, *Curr. Appl. Phys.* 9, 1434 (2009).
9. Y. Zeng, F. Yao, G. Zhang, S. Liu, S. Jiang, Y. Yu, J. He, L. Zhang, and J. Yi, *Ceram. Int.* 39, 3709 (2013).
10. G. Zhang, M. Li, H. Li, Q. Wang, and S. Jiang, *Energy Technol.* 6, 791 (2018). https://doi.org/10.1002/ente.201700622.
11. T. Yu, G. Zhang, Y. Yu, Y. Zeng, and S. Jiang, *Sens. Actuators A* 223, 159 (2015).
12. S. Kar-Narayan and N.D. Mathur, *J. Phys. D.* 43, 032002 (2010).
13. M. Ožbolt, A. Kitanovski, J. Tušek, and A. Poredoš, *Int. J. Refrig.* 40, 174 (2014).
14. M. Valant, *Prog. Mater Sci.* 57, 980 (2012).
15. B. Charlot, D. Coudouel, F. Very, P. Combette, and A. Giani, *Sens. Actuators Phys.* 225, 103 (2015).
16. M. Vaish, M. Sharma, R. Vaish, and V.S. Chauhan, *Integr. Ferroelectr.* 167, 90 (2015).
17. S.B. Lang, *Phys. Today* 58, 31 (2005).
18. G.Z. Zhang, S.L. Jiang, Y.K. Zeng, Y.Y. Zhang, Q.F. Zhang, and Y. Yu, *J. Am. Ceram. Soc.* 92, 3132 (2009).
19. K.S. Srikanth, V.P. Singh, and R. Vaish, *J. Eur. Ceram. Soc.* 37, 3943 (2017).
20. S. Patel, A. Chauhan, S. Kundu, N.A. Madhar, B. Ilahi, R. Vaish, and K.B.R. Varma, *AIP Adv.* 5, 087145 (2015).
21. S. Patel, A. Chauhan, and R. Vaish, *Solid State Sci.* 52, 10 (2016).
22. K.S. Srikanth, S. Patel, S. Steiner, and R. Vaish, *Appl. Phys. Lett.* 110, 232901 (2017).
23. K.S. Srikanth and R. Vaish, *J. Eur. Ceram. Soc.* 37, 3927 (2017).
24. S. Patel, A. Chauhan, S. Kundu, N.A. Madhar, B. Ilahi, R. Vaish, and K.B.R. Varma, *AIP Adv.* 5, 087145 (2015).
25. S.L. Jiang, P. Liu, X.S. Zhang, L. Zhang, Q. Li, J.L. Yao, Y.K. Zeng, Q. Wang, and G.Z. Zhang, *J. Alloys Compd.* 636, 93 (2015).
26. Y.Y. Zhang, G.S. Wang, T. Zeng, R.H. Liang, and X.L. Dong, *J. Am. Ceram. Soc.* 90, 1327 (2007).
27. B.P. Kumar, H.H. Kumar, and D.K. Kharat, *Mat Sci Eng B-Solid* 127, 130 (2006).
28. K.S. Srikanth, V.P. Singh, and R. Vaish, *Int. J. Appl. Ceram. Technol.* 15, 140 (2018).
29. T. Ohji and M. Fukushima, *Int. Mater. Rev.* 57, 115 (2012).
30. J. Roscow, Y. Zhang, J. Taylor, and C.R. Bowen, *Eur. Phys. J Spec. Top.* 224, 2949 (2015).
31. H.L. Zhang, J.F. Li, and B.P. Zhang, *Acta Mater.* 55, 171 (2007).
32. T. Zeng, X.L. Dong, C.L. Mao, Z.Y. Zhou, and H. Yang, *J. Eur. Ceram. Soc.* 27, 2025 (2007).
33. G. Suyal and N. Setter, *J. Eur. Ceram. Soc.* 24, 247 (2004).
34. Q. Zhang, S. Corkovic, C.P. Shaw, Z. Huang, and R.W. Whatmore, *Thin Solid Films* 488, 258 (2005).
35. S. Kumamoto, K. Mizumura, Y. Kurihara, H. Ohhashi, and K. Okuno, *Jpn. J. Appl. Phys.* 30, 2292 (1991).
36. S.B. Lang and D. Das-Gupta, *Handbook of Advanced Electronic and Photonic Materials and Devices* (San Diego: Academic Press, 2001), p. 235.
37. S. Yao, W. Ren, H. Ji, X. Wu, P. Shi, D. Xue, X. Ren, and Z.G. Ye, *J. Phys. D Appl. Phys.* 45, 195301 (2012).
38. G. Zhang, S. Jiang, Y. Zeng, Y. Zhang, Q. Zhang, and Y. Yu, *J. Appl. Phys.* 106, 034110 (2009).
39. P. Yu, Y.D. Ji, N. Neumann, S.G. Lee, H. Luo, and M. Es-Souni, *IEEE Trans. Ultrason. Ferr.* 59, 1983 (2012).
40. Y.X. Tang and H.S. Luo, *J. Phys. D Appl. Phys.* 42, 075406 (2009).
41. G. Singh, V.S. Tiwari, and P.K. Gupta, *Appl. Phys. Lett.* 103, 202903 (2013).
42. C.R. Bowen, J. Taylor, E. LeBoulbar, D. Zabek, A. Chauhan, and R. Vaish, Energ. *Environ. Sci.* 7, 3836 (2014).

43. R. Sun, J. Wang, F. Wang, T. Feng, Y. Li, Z. Chi, X. Zhao, and H. Luo, *J. Appl. Phys.* 115, 074101 (2014).
44. L. Xing, C. Zhihui, W. Dun, F. Bijun, D. Jianning, Z. Xiangyong, X. Haiqing, and L. Haosu, *Jpn. J. Appl. Phys.* 54, 071501 (2015).
45. C.R. Bowen, J. Taylor, E. Le Boulbar, D. Zabek, and V.Y. Topolov, *Mater. Lett.* 138, 243 (2015).
46. J. Zhang, X. Dong, F. Cao, S. Guo, and G. Wang, *Appl. Phys. Lett.* 102, 102908 (2013).
47. X. Liu, D. Wu, Z. Chen, B. Fang, J. Ding, X. Zhao, and H. Luo, *Adv. Appl. Ceram.* 114, 436 (2015).
48. Y. Zhang, Y. Bao, D. Zhang, and C.R. Bowen, *J. Am. Ceram. Soc.* 98, 2980 (2015).
49. H. Zhang, S. Jiang, and K. Kajiyoshi, *J. Am. Ceram. Soc.* 93, 1957 (2010).
50. A. Seifert, P. Muralt, and N. Setter, *Appl. Phys. Lett.* 72, 2409 (1998).
51. A. Seifert, L. Sagalowicz, P. Muralt, and N. Setter, *J. Mater. Res.* 14, 2012 (1999).